Advancements in Modeling and Analysis of Artificial Periodic Inhomogeneities in the Ionosphere

IRRI-7

bl639@cornell.edu

BRIAN LA ROSA[1], DAVID HYSELL[1]

[1]Cornell University

1. INTRODUCTION

The Artificial Periodic Inhomogeneities (API) are electron plasma density structures created by heating the ionosphere using powerful high-frequency waves emitted from ground-based facilities. These irregularities has been detected across the D, E and F regions, and the backscatter signals has been used to study a broad range of ionospheric phenomena (Bakhmetieva, 2022).

Many analytical approximations have been proposed to model the occurrence of API, but a unified model is still absent. In this work we focus on the following aspects:

1) Provide a brief review of the formation mechanisms of API structures for each of the ionosphere regions.
2) Present a 1D fluid model (Hysell et al., 2023) capable of reproducing the occurrence of API across the layers of the ionosphere.
3) Analyse the electron density structures obtained with this simulation.

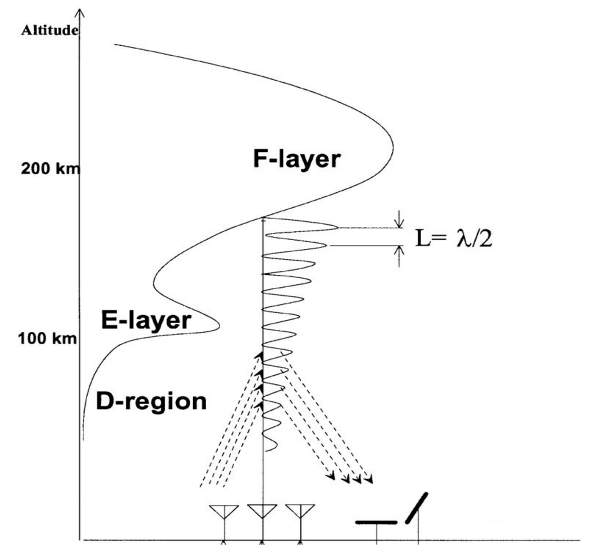

Figure 1: Conceptual diagram of a typical API experiment.

2. BACKGROUND

- **D-region:** At these altitudes, the negative ion chemistry has been reported as the formation mechanism of API structure. Local heating of the electron gas in the nodes of the powerful standing HF wave increases the rate of attachment of electrons to oxygen molecules, reducing the electron density and increasing the negative ion density of oxygen (Belikovich, 1999). The most relevant processes of electron attachment are listed in Table 1.

Attachment Reactions	Rate Coefficient ($cm^6.s^{-1}$)	Production ($m^{-3}s^{-1}$)
$O_2 + O_2 + e^- \xrightarrow{\beta_1} O_2^- + O_2$	$\beta_2 = 1.0\times10^{-31}.\left[\frac{300}{T_e}\right]^2.\, exp\left[-\frac{600}{T_e}\right]$	$R_1 = \beta_1.n_e.N_{O_2}^2$
$O_2 + N_2 + e^- \xrightarrow{\beta_2} O_2^- + N_2$	$\beta_2 = 1.0\times10^{-31}.\left[\frac{300}{T_e}\right]^2.\, exp\left[-\frac{70}{T_e}\right]$	$R_2 = \beta_1.n_e.N_{O_2}.N_{N_2}$

Table 1: Principal electron attachment reactions.

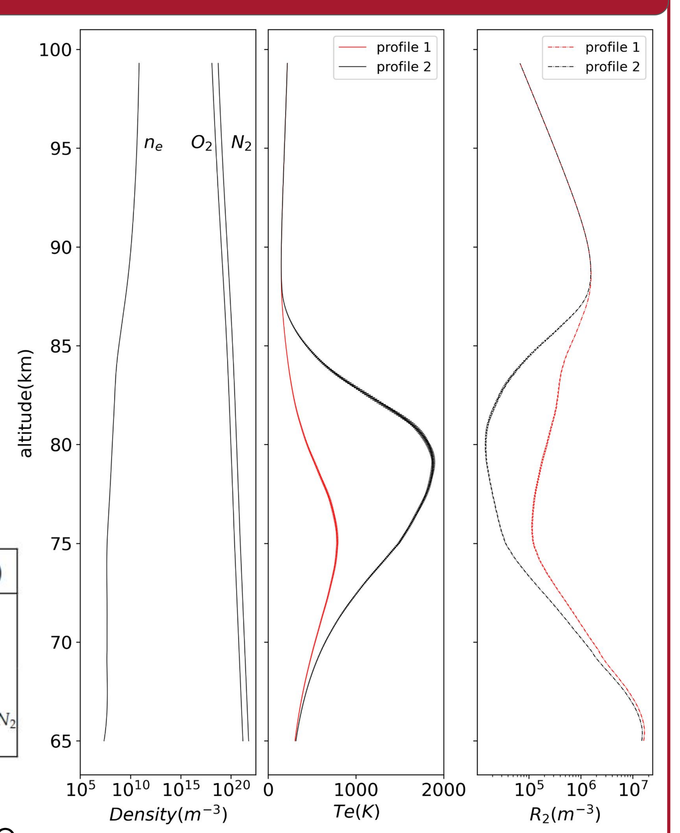

Figure 2: The left panel shows a typical e^-, N_2 and O_2 density profiles. The central panel shows two electron temperature profiles. The right panel shows the electron population lost by the second attachment process.

The right panel in Figure 2 illustrates the population of electrons lost due to the second attachment process, as detailed in Table 1, across various altitudes and two distinct temperature profiles. It is evident that the form of the rate coefficients significantly influences the electron density variations: at lower electron temperatures, these variations are more pronounced, whereas at higher temperatures, the variations are reduced.

- **E-region:** In this region, the diffusion of plasma species plays a crucial role in maintaining quasineutrality. Assuming a single main ion concentration we obtain the well known ambipolar diffusion coefficient. For two ion species, this diffusion is described by an eigenvalue problem that combines the linearized, one-dimensional continuity and momentum equations for the ion species and massless electrons, while imposing the quasineutrality condition (D. Hysell, 2014):

Decay Rate:

Ambipolar diffusion

$$D_j = \frac{k_B(T_e+T_j)}{M_j\nu_{nj}} \qquad \tau = \frac{1}{2k^2D_j}$$

Eigenvalues: $\{D_{min}, D_{max}\}$

Multipolar diffusion

$$\begin{pmatrix}\partial_t n_1\\ \partial_t n_2\end{pmatrix} = \begin{pmatrix}(\frac{n_{o1}}{n_{oc}}+1)D_1 & \frac{n_{o1}}{n_{oc}}D_1\\ \frac{n_{o2}}{n_{oc}}D_2 & (\frac{n_{o2}}{n_{oc}}+1)D_2\end{pmatrix}\begin{pmatrix}\nabla^2 n_1\\ \nabla^2 n_2\end{pmatrix} \qquad \tau = \frac{1}{2k^2D_{min}}$$

The information provided here is relevant for the modelling because the relaxation of the API irregularities is expected to decay due to the diffusion of particle species when the heater is turned off, an serve as a benchmark in accordance with the expressions mentioned above.

- **F-region:** The external oscillatory electric field produced by the heater induce a response in the charged particles that acts to repeal them from the region of strongest field. This force is called the ponderomotive force and has been identified as the mechanism driving irregularity formation in the F region:

$$\mathbf{F}_{p,j} = -\frac{q_j^2}{4m_j\omega^2}\nabla(E_o^2)$$

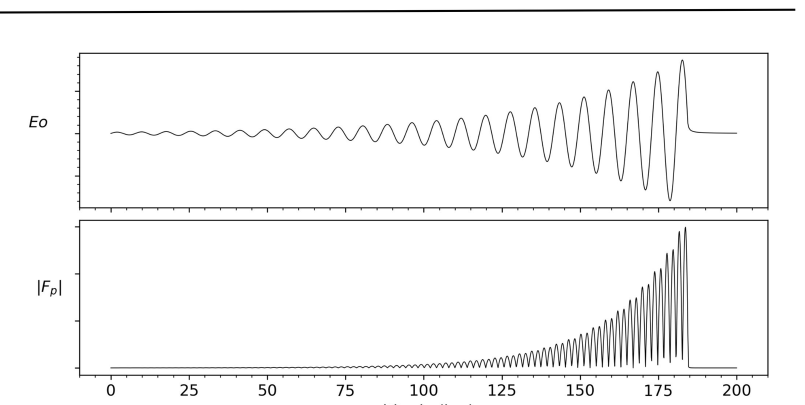

Figure 3: Illustration of the external electric field propagating through the ionosphere (top panel) and the associated ponderomotive force (bottom panel)

3. MODEL DESCRIPTION

- The model proposed is based on the low-latitude ionosphere model developed by Bailey and Balan, incorporating the effects of the heating wave and the formation mechanism of the API structures. The resulting equations, which are reduced to an altitude-dependent behavior, can be written as shown here.

Fluid equations:

$$\begin{cases}\frac{\partial n_j}{\partial t} + \nabla_z\cdot(n_jv_j) = \boxed{P_j - L_jn_j}\\ v_j = \frac{1}{m_j\nu_j}\left[q_jE - \frac{1}{n_j}\nabla_zp_j - \boxed{F_{p,j}}\right]\\ \frac{\partial T_e}{\partial t} - \frac{2}{3n_ek_B}\nabla_z\cdot(\hat{\kappa}_e\nabla_zT_e) = Q_{en}+Q_{ei}+\boxed{Q_{heat}}\end{cases}$$

$$Q_{heat} = \frac{|E_o(z)|^2}{Z_on_ek_B}\frac{\omega}{c}n_r(z)n_i(z)$$

Here n is the index of refraction

$$n_e = \sum_j q_jn_j$$

$$\nabla_z\cdot J = \sum_j q_j\nabla_z\cdot(n_jv_j) = 0$$

- In the continuity equation, P_j and L_j are the production and loss terms, respectively. For the momentum equation, we assume inertialess particles, and the pressure term is equal to p_j=kn_jT_j. In the energy equation, the κ_e corresponds to the thermal conductivity tensor, and Q_{heat} is the heating rate produced by the pump wave. The highlighted terms in red, along with the net zero current and quasineutrality condition, defined the proposed model for the formation of API irregularities.

- This set of equations has been solved for the following ion species O_2^+, NO^+, O^+, O_4^+, and O_2^-, using the Mitra-Rowe ion chemical scheme, which includes electron attachment reactions. Furthermore, the required computational tools and initial parameters for the simulation are listed in Table 2.

Initialization	- MSIS2: n^0, Ti - IRI2016: n^+, T_i,T - E(z): full wave solution of Stoke's equation (see Lundborg, 1986)
Computational tools	- Savitzky-Golay filter for n^+ species. - Finite differences discretization for fluid equations. - 2nd order Runge-Kutta solver for fluid equations.
Computational parameters	$\Delta z \rightarrow 22m$, $\Delta t \rightarrow 8\mu s$, $\omega \rightarrow 4.4$MHz

Table 2: Required parameters and computational tools

- A small time step has been used. However, this is justified by the rapid formation of API irregularities (< 1 sec), requiring only a moderate number of iterations. In order to collapse the time evolution of the API processes, the electron and ion temperature equations are advanced 8 μs whereas the ion continuity equations are advanced 200 times faster - 1.6 ms per iteration. This choice preserves a distinct separation of timescales while permitting practical and expedient simulation runs (Hysell, 2023).

4. RESULTS

- The plasma temperature and density perturbations induced by the HF pump wave induced miniscule signals difficult to detect and visualize. An implementation of a more sensitive diagnostic match filter was made by correlating the electron density with the HF pump amplitude E_o, T_e and Ti. The resulting correlations can be noisy, but the peaks are used to determine the occurrence of API.

- Figure 4 shows the simulation results at the 400 timestep iteration. While electron density perturbations are not evident in the density plot (left panel), the correlation curve between n_e and E_o (rigth panel, black curve) exhibits several negatively correlated peaks at different altitudes. This behavior is expected due to the presence of an external electric field, which reduces electron density in regions where the amplitude is greater, as previously discussed in the background section.

- The RTI plot of the correlation between the electron density and the pump wave amplitude, shown in Figure 5, provides a clearer understanding of the formation of API irregularities simulated with the proposed model. As soon as the simulation begins (Q_{heat} >0), several peaks with varying correlation values appear and persist until the heater is turned off (indicated by the black vertical dashed line). After this point (Q_{heat} =0), the intensity of the correlation starts to decay, suggesting that there is no electron density perturbations are caused by the external electric field imposed by the heater.

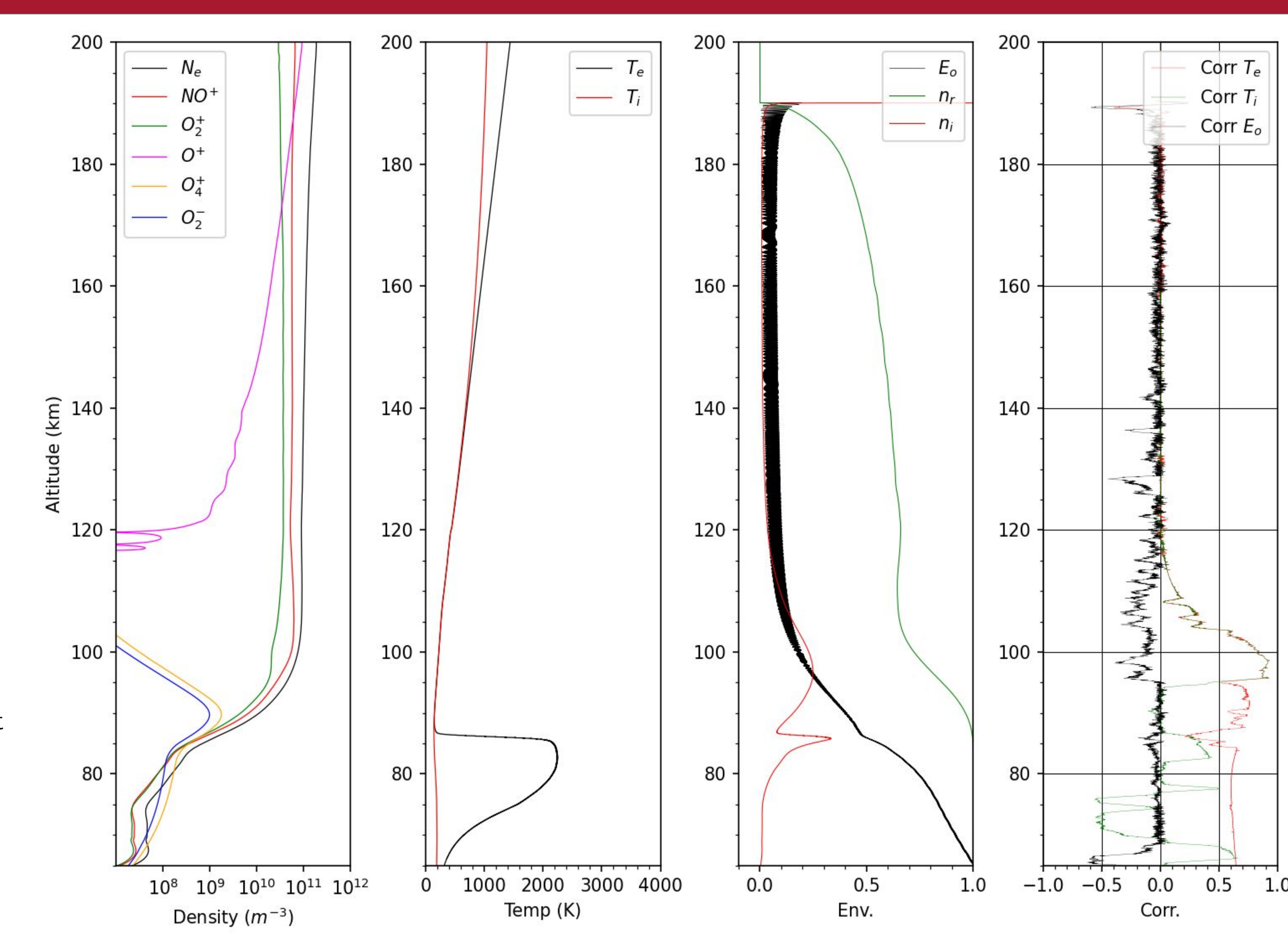

Figure 4: Results of numerical simulation at timestep 400. Left panel: Number density of electrons (black), NO^+ (red), O_2^+ ions (green), O^+(magenta), O_4^+(orange), and O_2^- (blue) versus altitude. Center left panel: Electron (black) and ion (red) temperature. Center right panel: Real part of the index of refraction (green), imaginary part of the index of refraction ×250 (red), and normalized HF pump mode amplitude envelope (black). Right panel: Correlation of electron density (black), electron temperature (red), andion temperature (green) with the HF pump mode envelope.

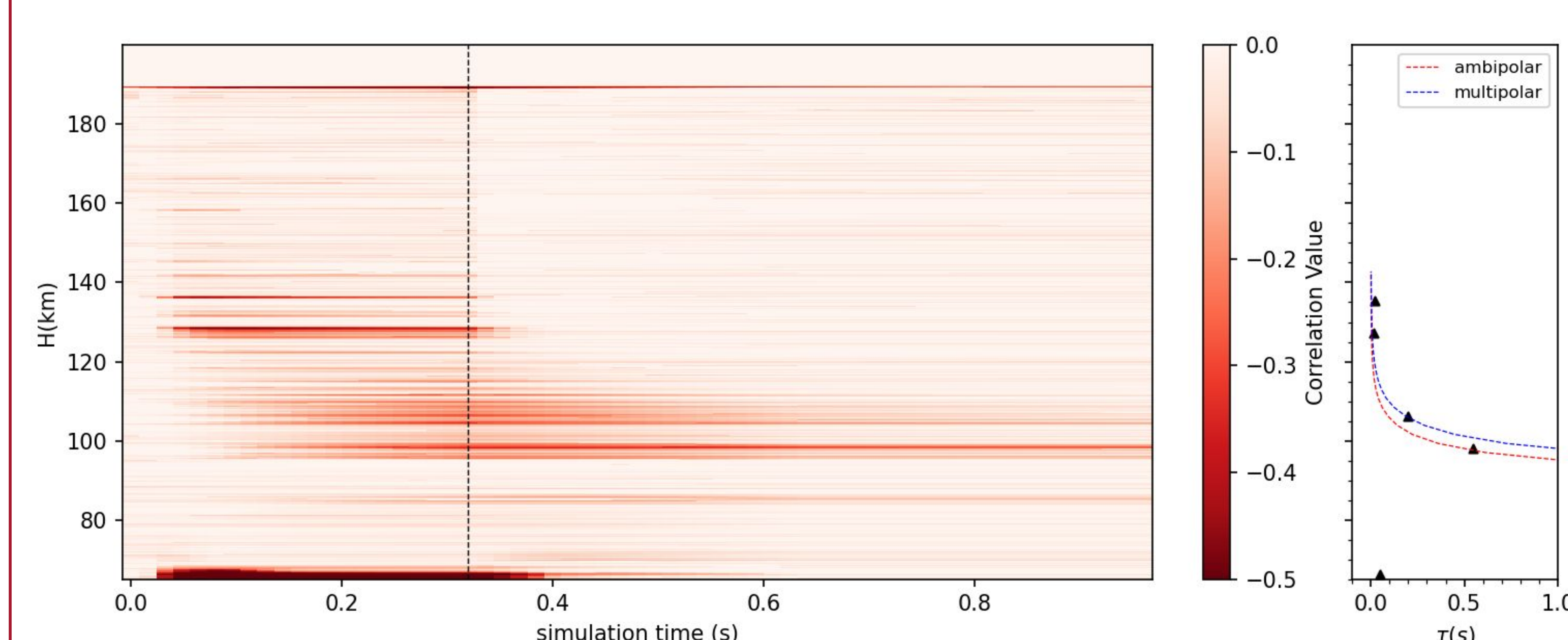

Figure 5: The left panel shows the RTI plot of the correlation between electron density and HF wave amplitude. The right panel shows the decay rate analysis of the of the main electron density perturbations after the heater is turned off (black triangles), in addition with the analytical decay rate approximation for ambipolar (red, single ion O_2^+) and ambipolar (blue, two ions: O_2^+, NO^+).

- In the right panel of Figure 5 ,the decay rates of the correlation for the the main peaks has been calculated by fitting curves of the form ~exp(-t/τ) .These estimates are in agreement with the values reported in the literature (see references 4, 6, and 7) and with both theoretical approximations, except for the D region correlation peak where the validity of these approximations is lost.

Altitude (km)	Decay rate $\tau(s)$
67.6	0.05
98.5	0.58
107.4	0.23
128.0	0.04
136.3	0.02

Table 3: Decay rates values for main correlation peaks.

- The results show that the mechanisms included in the model were sufficient to reproduce the formation of API irregularities. While we understand the mechanisms driving these perturbations, predicting the exact location of API formation is challenging due to the complexity of other physical interactions.

5. CONCLUSIONS

- A brief review of the formation mechanisms of API structures was provided for each ionospheric region, including the physical interactions between the pump wave and the plasma
- The integration of these formation mechanisms into a one-dimensional fluid model was presented, along with the computational parameters used.
- The simulation results demonstrate that the typical behavior of API irregularities was successfully reproduced for each ionospheric region. Information about the decay of these irregularities was also provided, showing agreement with the literature.
- Further analysis is required to build a better diagnosis that permits an accurate proxy for the backscatter signal-to-noise ratio.

6. REFERENCES

1. Bailey, G. J., & Balan, N. (1996). A low-latitude ionosphere-plasmasphere model. In R. W. Schunk (Ed.), STEP: Handbook of ionospheric models(pp. 173–206). Utah State University.
2. Bakhmetieva N. & Grigoriev G (2022)., Study of the Mesosphere and Lower Thermosphere by the Method of Creating Artificial Periodic Irregularities of the Ionospheric Plasma. https://doi.org/10.3390/atmos13091346
3. Blaustein, N. & Photoniuc, E. (2007). *Ionosphere and Applied Aspects of Radio Communication and Radar.*
4. Belikovich, V. V., Benediktov, E., & Tolmacheva, A. V. (1989). *Diagnostics of parameters of the ionospheric plasma in the F-region by the method of resonance scattering by artificial periodic inhomogeneities.* Geomagnetism and Aeronomy, 237–240.
5. Belikovich, V.V., Benediktov, E.A., Bubukina, V.N. et al. *Artificial periodic inhomogeneities and a model for the lower part of the D region.* Radiophys Quantum Electron 42, 382–387 (1999). https://doi.org/10.1007/BF02677617
6. Hysell, D. L. et. al. (2014). *First artificial periodic inhomogeneity experiments at HAARP.* Geophysical Research Letters .https://doi.org/10.1002/2015GL063064
7. Hysell, D. L., & Rojas, E. (2023).*Modeling E-Region Artificial Periodic Inhomogeneity.* Radio Science. https://doi.org/10.1029/2023RS007710
8. Lundborg, B. et al (1985). *Standing wave pattern of HF radio waves in the ionospheric reflection region: 1. General Formulas.* Radio Science. https://doi.org/10.1029/RS020i004p00947